Developing High-Pressure, Solid-State Experiments on the Nova Laser

D. H Kalantar *A. A. Hauer*[*] *J. S. Wark*[††]

E. A. Chandler *M. A. Meyers*[†] *S. V. Weber*

J. D. Colvin *K. O. Mikaelian* *L. G. Wiley*

D. M. Gold *B. A. Remington*

Introduction

In a classical fluid model, when a light fluid accelerates a heavier fluid, the interface is Rayleigh–Taylor (RT) unstable. As a result, any mass modulation at the embedded material interface is unstable and can grow when accelerated. However, when a material is in the solid state, the strength of the material can counter the effect of the RT instability. The parameters that define whether a material is stable or unstable and undergoes instability growth in the solid state depend on the wavelength and amplitude of the modulation, acceleration history, foil thickness, and material properties, such as yield stress and shear modulus.

Solid-state instability growth will occur in the plastic flow regime. Plastic behavior is described by a semi-empirical constitutive model[1] that has been developed for phenomena that occur at strain rates $<10^5$ s^{-1}. Such plastic flow has been characterized either microscopically by the theory of lattice dislocations, or macroscopically by an effective lattice viscosity.[2] The best approach to describe the plastic flow of a material may depend on the specifics of a particular experiment. Neither approach has been well tested experimentally at pressures over 1 Mbar or strain rates $>10^8$ s^{-1}.

Analytically, stability boundaries can be defined, as described by Lebedev et al.[3,4] Such boundaries can be used to determine whether material strength is sufficient to inhibit plastic deformation, completely stabilizing growth of a modulation. Outside the stability boundary, the material may undergo plastic deformation, and the modulated interface may grow. Such deformation and growth have been demonstrated by Barnes et al.[5] using Al plates with a preimposed surface modulation, where the plates are driven with a high-explosive drive, and by Lebedev et al.[3,4] using Al and Ti plates in similar experiments.

We are conducting experiments on the Nova laser[6] to study the plastic flow of metals at high pressure and very high strain rates (10^7 to 10^8 s^{-1}). Our experiments are designed to compress Cu foils by a factor of 1.5 to 2.0 with staged shocks reaching peak pressures of about 3 Mbar. The RT instability is the observable "probe" in such experiments, with departures from classical (liquid) behavior characterizing the material-strength properties at high pressure and compression.

In this paper, we present details of the hohlraum target design and x-ray drive characterization for the Cu foil experiment. We also present calculations of the material state with this drive, and results from preliminary instability growth experiments using Cu foils with a preimposed modulation. With an accurate determination of the actual drive history, the Cu foil is calculated to melt on decompression, but the instability growth is calculated to be similar for Cu both as a solid and a fluid. We discuss the stability boundaries for solid-state plastic flow for the Nova experiments and conclude with a discussion of an improved experimental design using an Al foil, where the foil remains solid throughout the experiment, and strength effects should be considerably enhanced.

Experimental Details

The hydrodynamics experiments are conducted using an x-ray drive created in a cylindrical Au hohlraum. This x-ray drive accelerates a metal foil payload by ablation of a brominated polystyrene ablator layer. A preimposed sinusoidal modulation is located on the metal foil at the embedded interface. The growth of the RT-unstable interface is then diagnosed by face-on x-ray radiography using a gated x-ray framing camera.[7]

[*]Los Alamos National Laboratory, Los Alamos, NM
[†]University of California at San Diego, La Jolla, CA
[††]Department of Physics, Clarendon Laboratory, University of Oxford, Oxford, UK

Figure 1 shows the target geometry. The hohlraum (Figure 1a) is cylindrically symmetric with internal shielding to prevent hard x rays from preheating the Cu foil due to M-band emission coming from the laser spots on the inner hohlraum wall. The hohlraum is 3.44 mm in diameter and 5.75 mm long. The laser entrance holes are 1.2 mm in diameter, and the holes in the internal shields are 1.6 mm in diameter.

The hydrodynamics package shown in Figure 1b is mounted on the side of the hohlraum. It consists of a 20-μm-thick brominated polystyrene [CH(Br)] foil pressed in contact with the metal foil. The CH(Br) ablator has a 3% atomic Br fraction to enhance opacity to soft x rays. We typically use 18- to 19-μm-thick, oxygen-free, high-conductivity Cu foils that have been rolled and then machined to have a sinusoidal modulation.

Eight Nova beams generate an x-ray radiation environment in the two laser-heated cavities of the target. Reemitted x rays that pass through the holes in the internal shields heat the central (x-ray–heated) cavity and ablate material from the CH(Br) ablator, launching a series of shocks into the package. Without the internal shields, the 2- to 4-keV Au M-band component of the spectrum of emission from the laser plasmas would be absorbed throughout the full volume of the package, potentially preheating the Cu foil and causing it to melt and decompress. With internal shielding, the x rays incident on the ablator are generated by reemission from the regions of the wall that are not directly illuminated by the laser beams. The spectrum of these x rays is nearly Planckian, without a significant M-band component.

The x-ray drive ablates the brominated plastic, launching a series of shocks into the metal foil, compressing and accelerating it away from the hohlraum. We diagnose the growth of the perturbed, unstable, embedded interface by x-ray radiography using a large-area (0.7-mm-diameter focal spot) backlighter. The backlighter is generated with two additional Nova beams aligned to a separate Fe backlighter foil generating He_α x rays at 6.7 keV. A 2- to 3-ns, square laser pulse shape was used for these backlighter beams, and delays relative to the drive beams ranged from 5 to 14 ns.

X-Ray Drive Measurement

The laser pulse shape is designed to generate an x-ray drive that launches two shocks, compressing the Cu foil to a peak pressure of about 3 Mbar while maintaining the metal foil in the solid state. This pulse shape is shown in Figure 2. It has a peak-to-foot intensity ratio of about 30. We have characterized the x-ray drive using the Dante diagnostic[8] and side-on foil trajectories.

The Dante diagnostic is a filtered array of absolutely characterized x-ray diodes. The diodes are positioned to view the spectral soft–x-ray emission from the inner wall of the central section of the hohlraum through a Be-lined diagnostic hole. With the high-contrast shaped laser pulse, only the lowest energy channels of the Dante detected signals, starting at about 1.0 ns. The absolute signal levels from these diodes were used to estimate the Planckian drive temperature, which started at about 15 eV and rose to 40 eV at 3.5 ns. At temperatures greater than 40 eV, enough channels recorded signals that a spectral unfold could be performed. The measured radiation temperature rose from 40 eV at 4.0 ns to 90 eV at the end of the laser pulse at 6.5 ns, and then slowly decayed as energy was lost into the hohlraum walls and through the laser entrance holes.

The measured drive temperature in Figure 2 is shown along with the laser pulse shape. Note that the

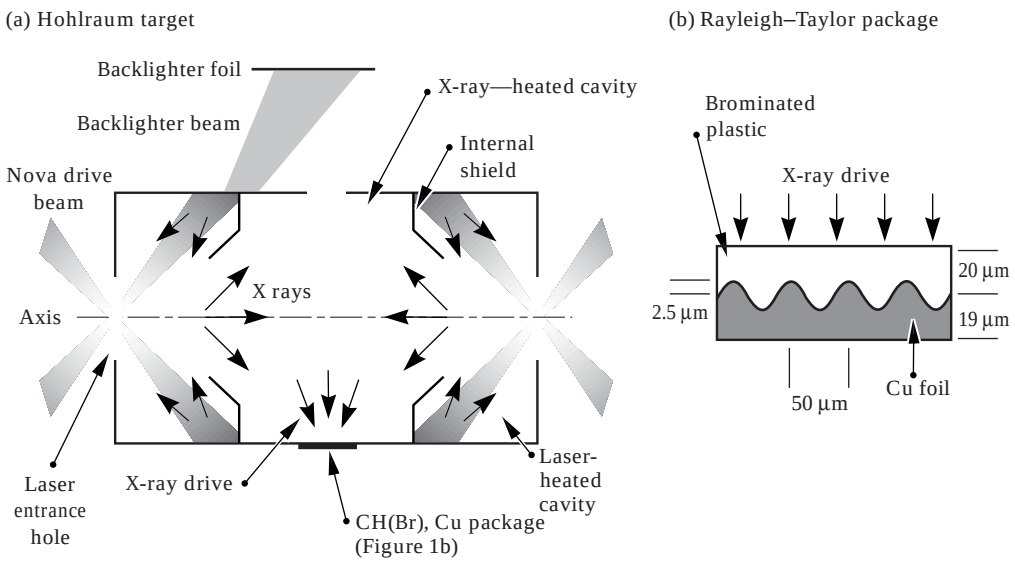

FIGURE 1. (a) Schematic of the internally shielded hohlraum and geometry for face-on radiography. (b) Modulated foil package mounted on the side of the hohlraum.
(08-00-1198-2247pb01)

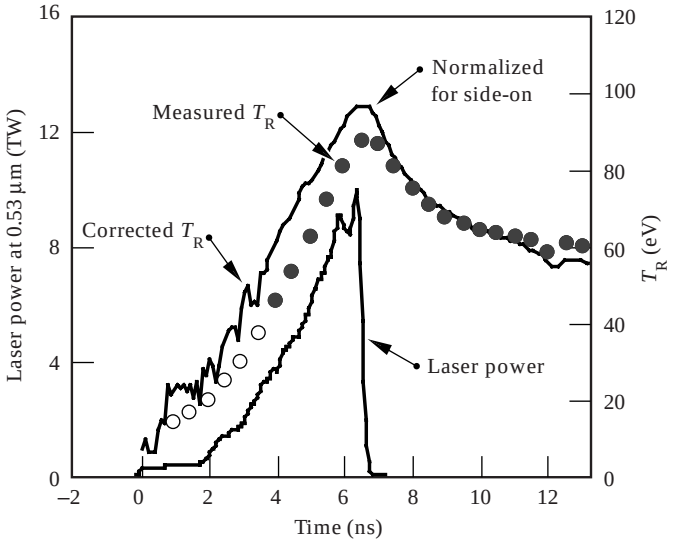

FIGURE 2. Laser pulse shape and x-ray drive temperature for the low-isentrope drive. (08-00-1198-2248pb01)

Dante measures the reemission from the wall of the hohlraum at the midplane. The package experiences the x-ray drive that is incident on the wall, the incident flux temperature T_I, which is related to the measured reemission flux temperature T_R by the albedo[9] α of the wall according the equation:

$$T_I = T_R / \alpha^{1/4} \quad . \tag{1}$$

We performed a full simulation of the hohlraum target using the LASNEX computer code,[10] including the laser power incident in the laser-heated regions, to estimate the drive temperature at the package. This resulting corrected drive is shown in Figure 2. As a consistency check for the low-temperature foot portion of the pulse, we analytically solve the power-balance prescription from Rosen and Lindl.[11] We consider the power flow in the laser-heated and x-ray–heated cavities of the internally shielded hohlraum. The laser power that enters the laser-heated cavities is equal to the sum of the losses through the laser entrance hole, losses into the wall, and power flow into the x-ray–heated cavity. Similarly, the power flow into the x-ray–heated cavity is equal to losses to the hohlraum wall and losses out to the laser-heated cavities. Incorporating the temporal scaling of the wall albedo from high-power, 1-ns drive experiments, we estimate that the temperature of the foot at 1 ns is about 24 eV. The LASNEX-simulated drive is in good agreement with this scaling at 20 to 25 eV.

The peak portion of the drive was verified with a side-on foil trajectory measurement. For this measurement, we mounted a package consisting of 22-μm CH(Br) with 13-μm Cu on the side of the hohlraum. We recorded an x-ray shadow image of the foil as it was accelerated away from the hohlraum using a high-magnification (55×), x-ray streaked imager (Figure 3). To match the overall motion of the foil, the albedo-corrected drive is reduced in the simulations by only about 2% in radiation temperature T_R for times $t > 5$ ns. This adjustment is interpreted as a correction due to the uncertainty in the opacity of the ablator at low drive temperatures, and in the initial Dante drive measurement itself.

Using the simulated x-ray drive in the hohlraum, we modeled the conditions in the foil package with 1D LASNEX. Figure 4 shows the calculated temperature and pressure at the embedded ablator–Cu interface. The x-ray drive ablatively launches two shocks into the copper. The first shock arising from the low foot is about 0.4 Mbar in the Cu, and the second is 3 Mbar. Subsequent reflected shocks maintain the high pressure until about 8 ns. At about this time, the material

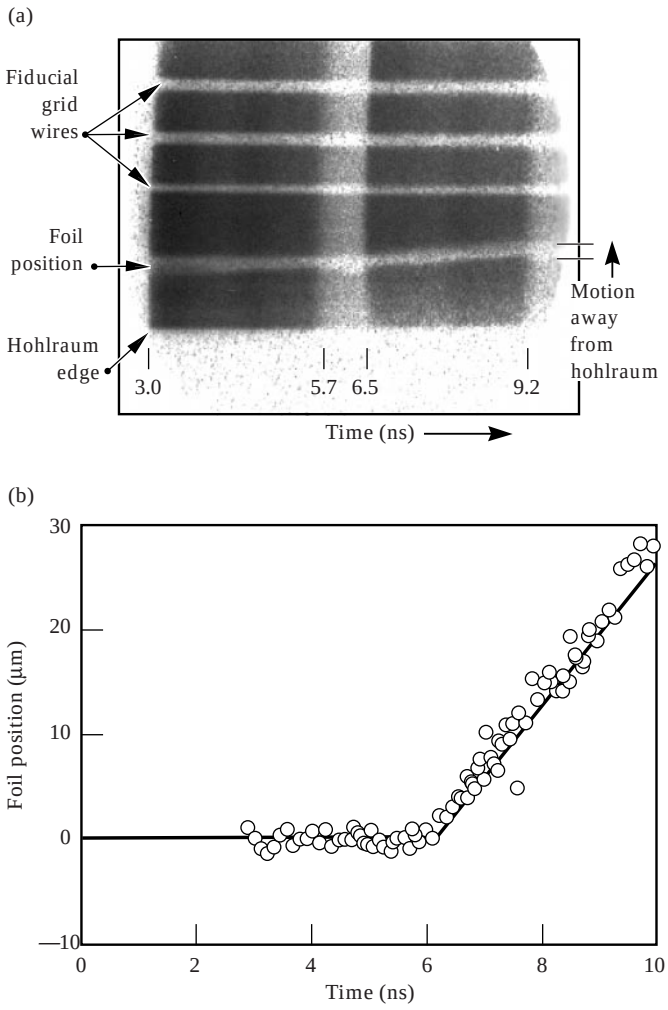

FIGURE 3. Side-on trajectory measurement for x-ray drive characterization. (a) Streaked data. (b) Measured trajectory of the rear surface of the target. (08-00-1198-2249pb01)

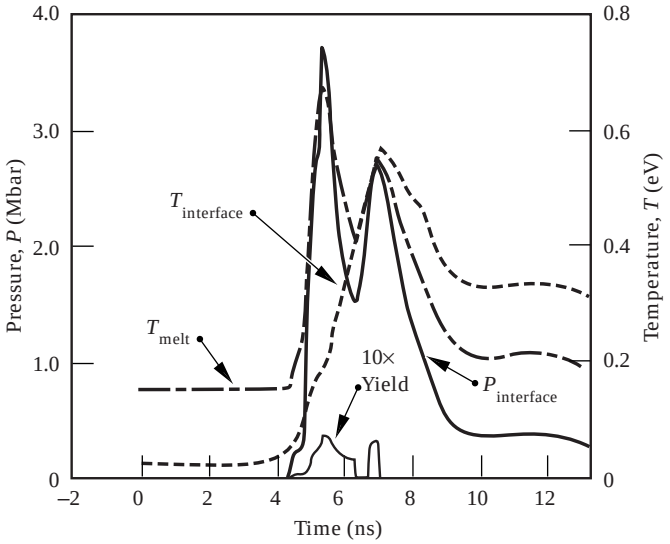

FIGURE 4. Pressure and temperature calculated at the CH(Br)–Cu interface with the low-isentrope drive. (08-00-1198-2250pb01)

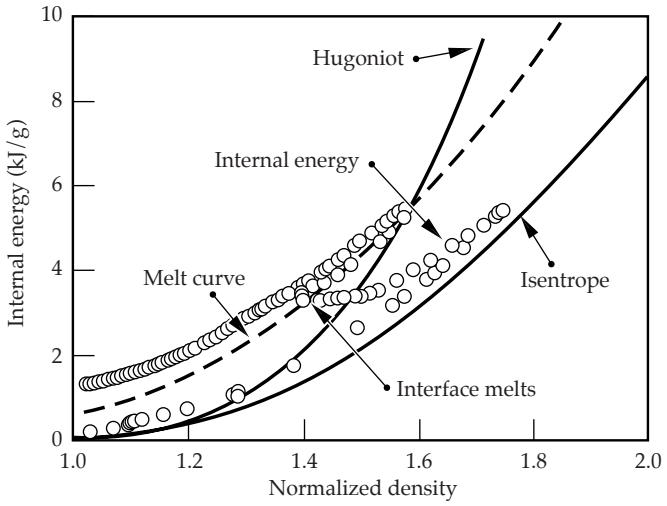

FIGURE 5. Internal energy trajectory of Cu at the CH(Br)–Cu interface for the low-isentrope x-ray drive. (08-00-1198-2251pb01)

temperature at the interface exceeds the melt temperature, which we calculate by the Lindemann law

$$T_m = T_{mo} \exp\left[2a\left(1-1/\eta\right)\right]\eta^{2\left(\gamma_0 - a - 1/3\right)} \ , \qquad (2)$$

where T_{mo} is the melt temperature at constant volume, η is the compression of the sample, γ is the Grüneisen gamma, and a is the coefficient of volume dependence of γ as defined by Steinberg et al.[1]

The low-isentrope drive is calculated to keep the foil very near an adiabat throughout the experiment. Figure 5 shows the internal energy at the Cu interface plotted as a function of density (compression) from $t = 0$ to $t = 15$ ns. Note that this trajectory is sensitive to the temperature of the foot of the shaped drive pulse. If the albedo correction for the foot is incorrect, the timing of the first shock may be incorrect. In particular, if the foot drive is much lower, then the second shock may catch up before it reaches the interface, placing the metal foil on a higher adiabat and potentially melting it. For the case of the actual drive, the shocks overlap about half way through the foil, melting the back side. The interface then melts with the rarefaction. Adjusting the level of the foot to be somewhat higher is one way to keep the temperature at the interface below the melt curve for longer times, as discussed later.

Experiments to characterize the foot drive were done using both active shock breakout[12,13] and dynamic Bragg diffraction techniques[14,15] to measure shock timing. For the active shock breakout measurement, we used a displacement Michaelson interferometer to measure motion of the back surface of a 17-μm-thick, Al flat target mounted on the side of the hohlraum. Motion of the back surface due to the shock transit and breakout through the foil is evident by a shift in the fringe pattern, as shown in Figure 6. Streaked interferometer data are shown in Figure 6a,

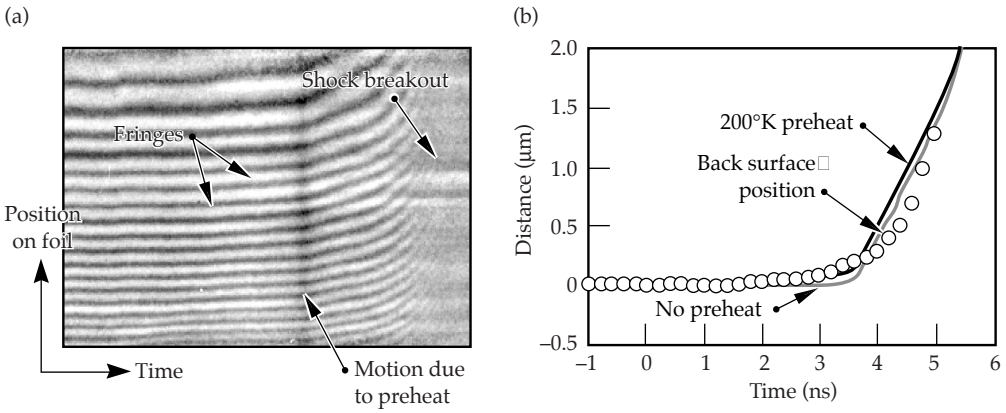

FIGURE 6. Displacement interferometer data showing the motion of the back surface of a 17-μm Al foil due to the shaped laser drive. (a) Streak data showing the fringes. (b) Reduced data shown with simulation. (08-00-1198-2252pb01)

and the analyzed position as a function of time for the back surface is shown in Figure 6b. This measurement was done with an interferometer that operates at a wavelength of 400 nm, so a full fringe shift corresponds to one-half wavelength (0.2 μm) of motion at the back surface.

The interferometer data show motion that may be due to the breakout of the elastic precursor wave or to some amount of preheat at the back surface of the Al foil, and then the rapid motion and disappearance of fringes as the main shock breaks out. We show simulated position as a function of time for the back surface with some imposed preheat to illustrate how this measurement is affected by low preheat levels.

For the case of Bragg diffraction, we used a CH(Br) ablator with a 40-μm-thick Si crystal as a surrogate for the Cu foil mounted on the side of the hohlraum. A V backlighter generated x rays at 5.3 keV, diffracting off the crystal through the brominated plastic ablator. When the shock transits the ablator and reaches the interface, it compresses the Si lattice. This is observed as a shift in the Bragg diffraction angle of the backlighter x rays. Figure 7 shows data obtained using this technique with a square laser pulse shape.[14–16] The estimated shock strength in the Si for this experiment was 350 kbar, compared to the calculated 650-kbar first shock strength in Cu for this shaped x-ray drive. Note that the presence of the diffraction signal under shock compression is consistent with the assumption that the Si remains solid under compression.

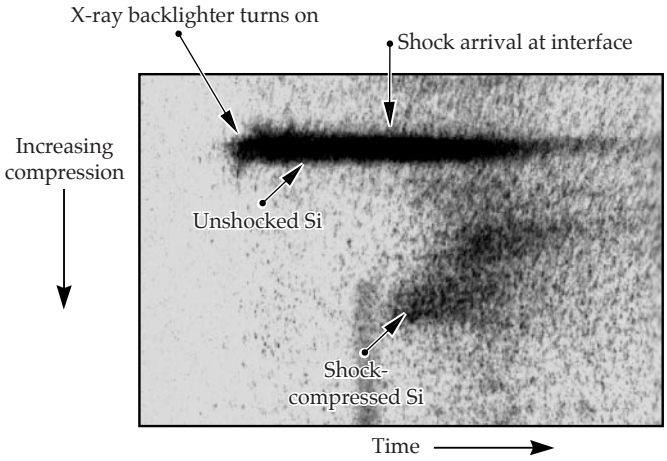

FIGURE 7. Streaked diffraction pattern from the CH(Br)–Si embedded interface showing a shift in the diffraction peak at the time the shock reaches the interface. (08-00-1198-2253pb01)

Instability-Growth Experiments

Sinusoidal modulations with amplitudes of 1.0 to 2.5 μm, and wavelengths of 20 and 50 μm, were machined in the Cu foils. A 20-μm thickness of brominated plastic ablator was pressed onto the modulated foils, and then the package was mounted over a hole in the side of the hohlraum. The x-ray drive ablatively launched a series of shocks to compress and accelerate the metal foil away from the side of the hohlraum.

We recorded radiographic images of the foil using 6.7-keV Fe x rays. Up to 16 images were recorded on four independently timed microchannel-plate striplines on each laser shot, using a flexible x-ray imager[17] with a 230-ps gate pulse. The modulation amplitude in optical depth was calculated by Fourier analysis at each time. The Fourier amplitude was normalized to the initial contrast in optical depth, which we measured on a separate shot.

Figure 8a shows the instability growth factors for $\lambda = 50$ μm, 2.5-μm-amplitude modulations; Figure 8b shows the growth factors for $\lambda = 20$ μm, 1.0-μm-amplitude modulations. In these experiments, the ablator–metal interface moved only about 40 μm during the time the measurements were made, and the overall growth factors were small, which means the modulation remained nearly linear. As a result, when we normalize the measurements with the initial (measured) contrast at that wavelength (x-ray mean-free-path and instrument resolution function), the instrument resolution (modulated transfer function ≈ 0.65 at 8× instrument

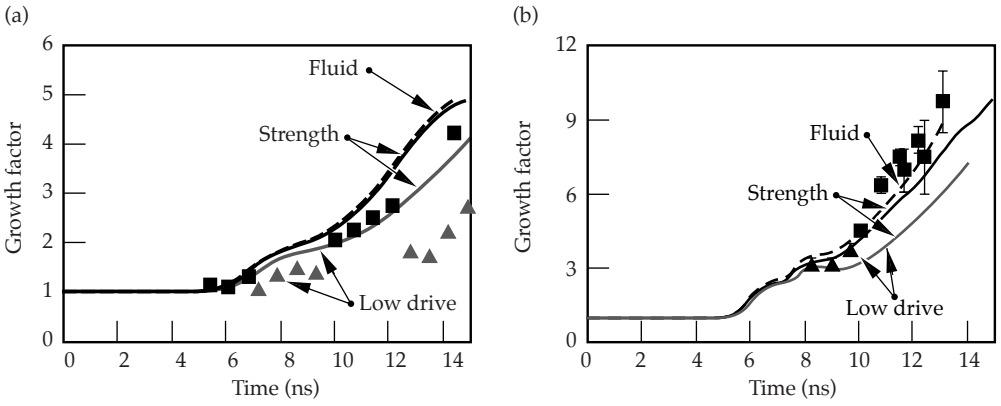

FIGURE 8. Instability growth factors for (a) 50-μm and (b) 20-μm wavelength modulation at the embedded CH(Br)–Cu interface. LASNEX simulations were done with and without strength. (08-00-1198-2254pb01)

magnification for $\lambda = 50$ μm, and 0.6 at 12× for $\lambda = 20$ μm) is removed from the measurement.

Figure 8 also shows the growth factors simulated with LASNEX using both a fluid model, and the constitutive material strength model described by Steinberg et al. Separate calculations are shown in Figure 8 for experiments where the peak portion of the laser pulse shape was reduced by about 20% (indicated on the figure by "low drive") because the growth is sensitive to the actual drive history. The difference between the fluid and material strength simulations for $\lambda = 20$ μm and 50 μm is small. For the 50-μm wavelength case, the simulations are nearly identical. For the 20-μm wavelength case, material strength leads to about 20% less growth, but the difference due to variation in the laser power history for the different shots is about this order, making it difficult to confirm that reduced growth is due to the material strength at $\lambda \geq 20$ μm with these Cu foils.

By extending the simulations to shorter-modulation wavelengths, $\lambda < 20$ μm, we observed a greater effect due to material strength. The calculated growth factors for a range of wavelengths from 5 to 50 μm are shown in Figure 9, plotted after the interface moved a distance of 20 μm. The enhanced difference between fluid and strength modeling at $\lambda \leq 20$ μm suggests that with some modifications we should be able to observe the effect of strength stabilization in the Nova experiments. Measuring perturbation growth factors at $\lambda = 5$ to 10 μm with gated pinhole imaging is problematic because of reduced exposure levels and diffraction effects with apertures smaller than 5 μm. As a result, this experiment would be improved with a design in which longer wavelengths would be stabilized.

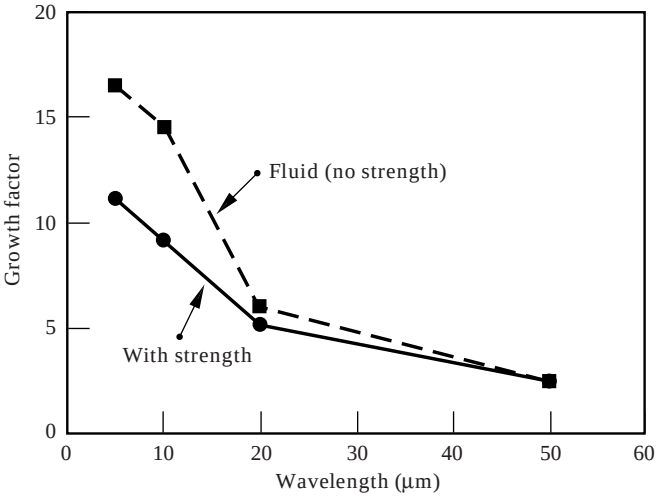

FIGURE 9. Growth factor as a function of wavelength for a modulated Cu foil, plotted after the interface moved a distance of 20 μm. (08-00-1198-2255pb01)

Strength Stabilization

The pressure-enhanced yield strength and shear modulus are given in the strain-rate-independent constitutive model by Steinberg et al. as

$$Y(P,T) = Y_0\left[1+\beta(\varepsilon+\varepsilon_i)\right]^n \times\left[1+\left(\frac{Y_P'}{Y_0}\right)\frac{P}{\eta^{1/3}}-\left(\frac{G_T'}{G_0}\right)(T-300)\right] \quad (3a)$$

and

$$G(P,T) = G_0\left[1+\left(\frac{G_P'}{G_0}\right)\frac{P}{\eta^{1/3}}-\left(\frac{G_T'}{G_0}\right)(T-300)\right] , \quad (3b)$$

where Y is the yield strength, G is the shear modulus, ε is the strain, and η is the compression. In this formulation, the pressure P and temperature T dependence and the effect of work hardening β are included. The initial value for yield strength is $Y_0 = 1.2 \times 10^{-3}$ Mbar, and the initial value for shear modulus is $G_0 = 0.477$ Mbar for a Cu foil.

At a shock pressure of 3 Mbar, the Cu foil is compressed by about a factor of >1.5, at which point the yield strength is 50 kbar, enhanced by a factor of about 40 over the nominal value Y_0. The shear modulus is about 3.6 Mbar. Under these conditions, the yield strength is exceeded by more than one order of magnitude, putting the foil into the plastic flow regime and allowing for instability growth in the solid state.

Estimates can be made as to whether the modulation on the Cu package grows or not, based on a stability boundary analysis assuming steady-state conditions. The Miles criterion, based on linear theory,[18] assumes a modulation amplitude η_0 much smaller than the wavelength. It establishes that for a semi-infinite slab with a modulated surface, the modulation is stable if its wavelength is shorter than the cutoff wavelength

$$\lambda_\infty = 4\pi G/\rho g \quad , \quad (4)$$

where g is the acceleration. Including the finite thickness of the foil, Lebedev et al. extend the Miles theory and predict this cutoff is at

$$\lambda_c = \frac{2\lambda_\infty}{1+\sqrt{1+8\sqrt{3}c^2/gH}} \quad , \quad (5)$$

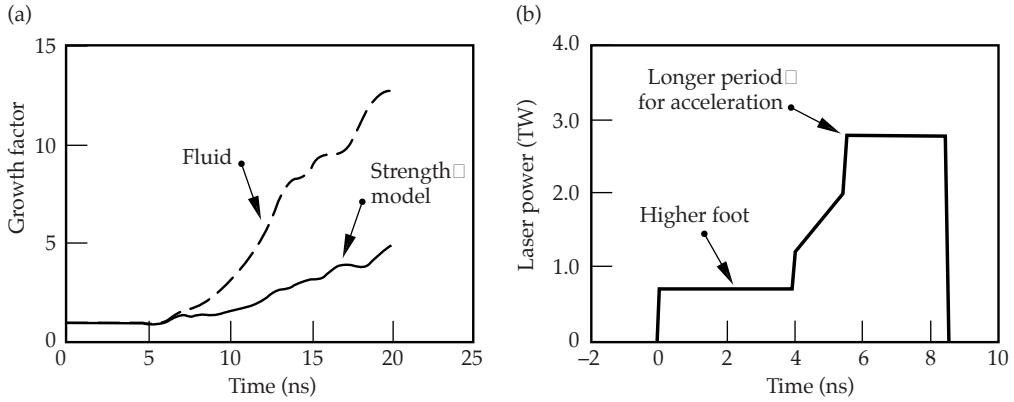

FIGURE 10. (a) Growth factor as a function of time, calculated for a modulated Al foil with a perturbation wavelength $\lambda = 20$ μm and initial amplitude of 0.5 μm. Simulations were done with and without material strength. (b) Laser pulse shape for the Al instability experiment. (08-00-1198-2256pb01)

where c is the speed of the shear wave, and λ_∞ corresponds to the Miles cutoff wavelength, Eq. 4. For the conditions of this experiment, $\lambda_c = 30$ μm. Therefore, at $\lambda = 20$ μm, which is below the cutoff wavelength, perturbations with very small initial amplitude under steady-state conditions should not grow.

We observed, however, that the $\lambda = 20$ μm modulation grows in both the experiment and the simulation. Growth results because the amplitude exceeds the critical amplitude given by Lebedev et al. This amplitude cutoff is given by the expression

$$\eta_c = \eta_c(\text{Drucker})\left[1 - 0.86e^{\left(2\pi H/\sqrt{3\lambda}\right)}\right] \times\left\{\left[1 - e^{\left(-2\pi H/\sqrt{3\lambda}\right)}\right]^2 - \left(\frac{\lambda}{\lambda_\infty}\right)^2\right\}, \quad (6)$$

where

$$\eta_c(\text{Drucker}) = \frac{2Y}{\rho g} \quad (7)$$

is the wavelength-independent critical amplitude threshold to instability growth from Drucker.[19] For these experiments, at $\lambda = 20$ μm, the amplitude threshold is <1 μm, which is much too small to diagnose by x-ray backlighting using a hard–x-ray backlighter at 6.7 keV.

To design an experiment in a regime with a much greater reduction in growth due to material strength, we must consider a material with a lower density and a larger value for the derivative of the yield strength with pressure to maximize the effect of strength on the RT instability growth. Aluminum is one such metal, with a pressure derivative of the yield strength that is a factor of 2 larger than that for Cu. For 7075 (or 6061) Al, which has an initial yield strength of 4.2 kbar, we calculated the growth of 20-μm wavelength with and without strength using an initial amplitude of 0.5 μm. The case with strength grows less than a factor of 2, whereas the fluid case shows a growth factor of about 5 at $t = 12$ ns (Figure 10a). Note that to time the shocks so that they do not overlap in the metal foil, the foot portion of the drive is raised and lengthened (Figure 10b). With this design, the peak pressure in the Al is 1.4 Mbar, and the foil is calculated to remain solid throughout, as indicated by a plot of the internal energy trajectory in Figure 11.

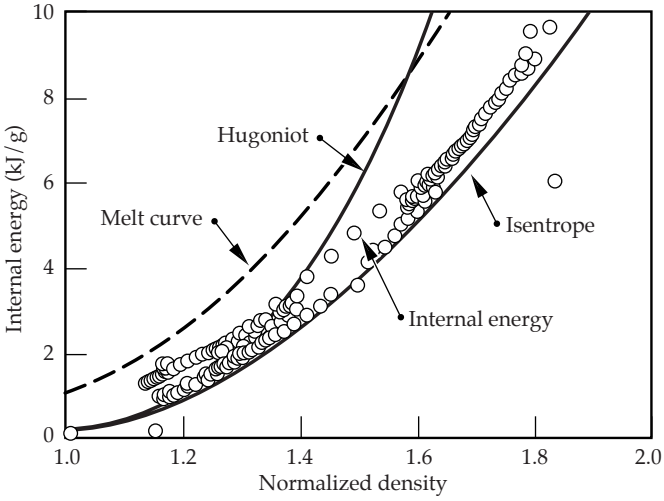

FIGURE 11. Internal energy trajectory calculated for an Al foil at the CH(Br)–Al interface. The modified drive is expected to shock the foil without melting it. (08-00-1198-2257pb01)

Summary

We have developed an x-ray drive to shock-compress metal foils in the solid state using an internally shielded hohlraum with a high-contrast shaped laser pulse. We used a combination of Dante measurements, side-on foil trajectories, and shock-timing measurements to develop an understanding of the x-ray drive. Hydrodynamic experiments that are designed to study growth of the RT instability in the plastic-flow regime have been started. Measurements of initial 20- to 50-μm wavelengths and 1- to 2.5-μm amplitude perturbations are presented and compared with simulations in this paper. For this experiment, the growth of the instability in fluid and solid states were calculated to be nearly the same. Analytic stability analysis is consistent with the instability growing in the plastic-flow regime. However, by redesigning the experiment to use an Al foil, the foil will remain in the solid state throughout, and the effect of material strength may be enhanced considerably, allowing us to conduct experiments on either side of the stability boundary.

Acknowledgment

We acknowledge the technical support of the Nova Operations and Target Fabrication groups at Lawrence Livermore National Laboratory.

Notes and References

1. D. J. Steinberg, S. G. Cochran, and M. W. Guinan, *J. Appl. Phys*. **51**, 1498 (1980).
2. L. C. Chhabildas and J. R. Asay, *J. Appl. Phys*. **50**, 2749 (1979).
3. A. I. Lebedev, P. N. Nizovtsev, and V. A. Rayevsky, in *Proceedings of the 4th International Workshop on the Physics of Compressible Turbulent Mixing*, 29 March–1 April, 1993 (Cambridge University Press, Cambridge, England, 1993), p. 81.
4. A. I. Lebedev, P. N. Nizovtsev, V. A. Rayevsky, and V. P. Soloviov, in *Proceedings of the 6th International Workshop on the Physics of Compressible Turbulent Mixing*, 17–21 June, 1997 (I.U.S.T.I./C.N.R.S., Marseille, France, 1997).
5. J. F. Barnes, P. J. Blewett, R. G. McQueen, K. A. Meyer, and D. Venable, *J. Appl. Phys*. **45**, 727 (1974).
6. E. M. Campbell, J. T. Hunt, E. S. Bliss, D. R. Speck, and R. P. Drake, *Rev. Sci. Instrum*. **57**, 2101 (1986).
7. P. M. Bell, J. D. Kilkenny, G. Power, R. Bonner, and D. K. Bradley, in *Ultrahigh Speed and High Speed Photography, Photonics, and Videography '89* (SPIE, Bellingham, WA, 1989), *Proc. SPIE*, Vol. 1155, pp. 430–444.
8. H. N. Kornblum, R. L. Kauffman, and J. A. Smith, *Rev. Sci. Instrum*. **57**, 2179 (1986).
9. R. L. Kauffman, H. N. Kornblum, D. W. Phillion, C. B. Darrow, B. F. Lasinski, L. J. Suter, A. R. Thiessen, R. J. Wallace, and F. Ze, *Rev. Sci. Instrum*. **66**, 678 (1995).
10. G. B. Zimmerman and W. L. Kruer, *Comments Plasma Phys. Controlled Fusion* **2**, 51 (1975).
11. J. Lindl, *Phys. Plasmas* **2**, 3933 (1995).
12. K. S. Budil, P. Celliers, G. W. Collins, L. B. Da Silva, R. Cauble, R. J. Wallace, G. Chiu, and A. Ng, in *Inertial Confinement Fusion Quarterly Report* **7**(1), UCRL-LR-105821-97-1 (1997); copies available from the National Technical Information Service, Springfield, VA.
13. G. W. Collins, P. Celliers, L. B. Da Silva, R. Cauble, D. Gold, M. Foord, K. S. Budil, R. Stewart, N. C. Holmes, M. Ross, B. A. Hammel, J. D. Kilkenny, R. J. Wallace, and A. Ng, *Phys. Plasmas* **5**, 1864 (1998).
14. Q. Johnson, A. Mitchell, R. N. Keeler, and L. Evans, *Phys. Rev. Lett*. **25**, 1099 (1970).
15. J. S. Wark et al., *Phys. Rev. B* **35**, 9391 (1987).
16. D. H. Kalantar et al., accepted for publication in *Rev. Sci. Instrum*. (to appear in Jan 1999).
17. K. S. Budil et al., *Rev. Sci. Instrum*. **67**, 485 (1996).
18. J. W. Miles, Technical Report No. GAMD-7335, General Dynamics, San Diego, CA (1966).
19. D. C. Drucker, *Ingenieur-Archiv* **49**, 361 (1980).